analytical chemistry

pubs.acs.org/ac Article

Competitive Delocalized Charge Transfer Boosted by Solvent Induction Strategy for Survivable Colorimetric Detection of ng-Level Urea

Xiaoyun Hu,[#] Tianshi Zhang,[#] Jiguang Li, Zhiwei Ma, Da Lei, Baiyi Zu, and Xincun Dou*

Cite This: *Anal. Chem.* 2022, 94, 6318−6328 Read Online

ACCESS | Metrics & More | Article Recommendations | Supporting Information

ABSTRACT: Achieving sensitive and robust colorimetry is of great significance for on-site chemical detection, but has always been a dilemma or at the expense of practicality. Here, from the perspective of solvent, which is commonly the indispensable medium for chemical sensing, the solvent induction strategy concerning the hydrophobic shielding and hydrophilic bonding solvent cage was proposed considering the configuration branching ratio in the reagent and the prevention of the autoxidation channel. Due to the competitive delocalized charge transfer in the probe and the effective viscous drag in the reagent, remarkable sensing signal concentrating and moisture retention capability were achieved. We expect the present strategy would facilitate the active but robust chemical reaction design and provide a universal methodology for the exploration of high-performance chemical sensors.

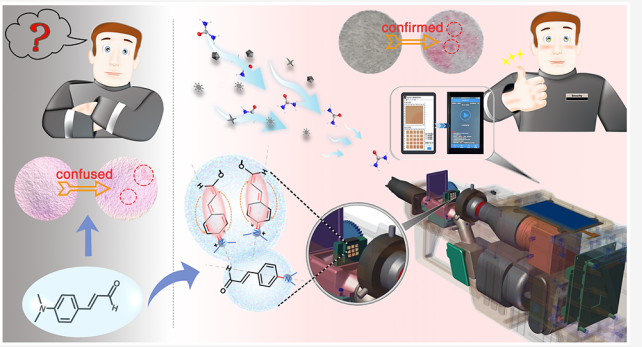

Colorimetry, which is generally highly specific, cost-effective, easy operation, and of quick and visual result, is one of the most intriguing topics in on-site chemical detection and has emerged broad applications biomedicine diagnosis,[1−3] environmental monitoring,[4,5] food safety,[6−8] explosive identification,[9−11] and so on. Since the first report on colorimetry, a series of novel probe molecules based on various reaction principles have been designed, such as cyclization reaction,[12−14] nucleophilic reaction,[15−17] oxidation reaction,[18−20] coordination reaction,[21−23] and so on, which laid a solid foundation for specific colorimetric recognition and the differentiation of analytes with similar properties/structures. There is no doubt that the development of high-performance probe molecules is the core of colorimetric sensing, and a series of probes were committed to improving the reaction efficiency, reducing reaction energy and improving the clarity of response signal through structure modification or new structure design.[24−26] However, the medium of the reaction taking place, which determines the reaction condition of the probe and the target analyte, as well as the practical sensitivity, is also pivotal. Especially in trace solid residue or airbone microparticulate analysis for nonvolatile improvised explosives or drugs,[27−30] the chemical sensing could only be realized by adopting solid−liquid reaction with desirable fast reaction and explicit color signal, whereas two severe constraints for choosing the reaction medium would be imposed. One is the long-term stability of the probe would face challenges from the liquid environment resulted undesired activity, and the other is the inevitable transport and diffusion of either the solid analyte or the reaction product would cause a fatal dilution of the limited color signal. In terms of the above issues, various mediums have been investigated, such as paper strips,[31,32] fibrous membranes,[33,34] hydrogels,[35−37] and so on, mainly focusing on solving the second challenge. However, no matter what kind of materials or technologies applied for solid−liquid type sensing, remarkably fundamental and crucial role of solvent should not be neglected.

The selection of solvent is of crucial importance to propose a chemical reaction because most chemical reactions essentially involve solution-phase chemistry,[38,39] and solvent might even play a decisive role in determining whether a chemical reaction could happen. Although solvents could be generally classified according to their physical properties, chemical properties, protophilic ability, chemical bond types,[40] and so on, for the convenience of intuitively expressing solvent−solute interaction, polarity comprising polar protic, dipolar aprotic and apolar,[41] could be the most influential factor to select a solvent in a specific chemical reaction. For different reaction systems, the selection of solvents could be distinguishable considering

Received: January 29, 2022
Accepted: April 6, 2022
Published: April 15, 2022

https://doi.org/10.1021/acs.analchem.2c00505
Anal. Chem. 2022, 94, 6318−6328

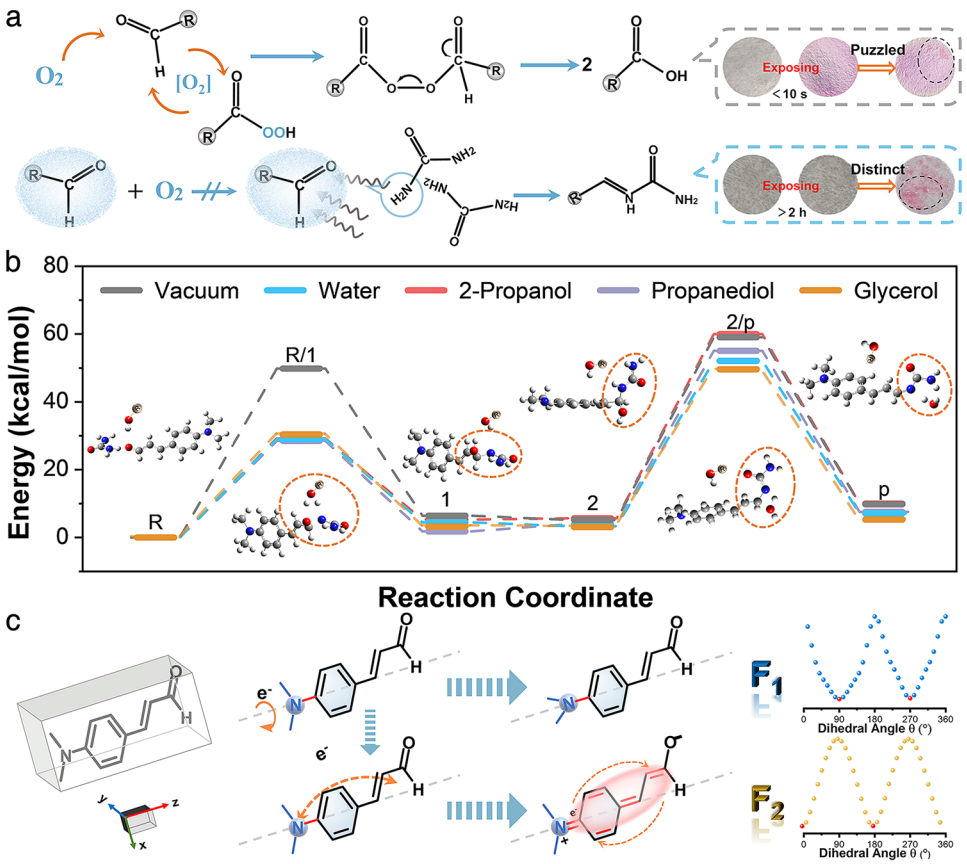

Figure 1. (a) Schematic illustration and diagram of the autoxidation in exposure environment and the solvent blocking effect in propanediol-glycerol solvent for *p*-DMAC and the corresponding reaction phenomenon. (b) The transition state analysis of the reaction process between *p*-DMAC and urea in vacuum and different solvents (water, 2-propanol, propanediol, glycerol). (c) The main configuration analysis of *p*-DMAC and the corresponding potential energy surface scan at dihedral angle (Formation 1: F_1; Formation 2: F_2).

the reaction solubility, reaction activity, reaction conditions, reaction direction, reaction products, and so on. A representative example employing a polar solvent (*N*,*N*-dimethylformamide) to form intermolecular hydrogen bond with sulfur atoms in colorimetric identification of polarity-lacking elemental sulfur shows the effectiveness of solvent polarity to the detection profermance.[42] Considering the solubility of TNT, DNT, $KMnO_4$, and S as well as the demand for high activity of the overall reaction system, a one-to-multi reagent with DMSO, toluene, and water as solvent combined with potassium isopropanol and urea was proposed to realize the one-step instantaneous visual detection of them.[43] A series of research show that solvent effect could determine the priority of mononuclear or binuclear substitution reaction,[44] improve the chelate cooperativity in coordination reaction,[45] transfer protons, and electrons to increase the reaction rate and product selectivity[46] due to various synergic effect between solvent and solute. Solvent effect could also directly change the structural characteristics of solutes and has been proven that the use of organic solvents can alter the solvation degree of the initial states and the transition states for dehydration reactions to achieve the high rate of acid catalytic reaction in liquid phase and improve selectivity.[47] However, whether solvent-induced design can be explored to maintain the reaction activity and ensure the stability and thus for the design of sensitive and survivable colorimetric sensing systems still remains unknown.

Herein, an efficient solvent induction strategy involving hydrophobic shielding and hydrophilic bonding solvent cage was designed to boost competitive delocalized charge transfer in quinone resonant *p*-dimethylaminocinnamaldehyde (*p*-DMAC) and was visualized by highly survivable and endurable sensing toward urea. The colorimetric detection and solid−liquid reaction modes offer an intuitive window to evaluate the reaction robustness and interfacial mass transfer process, and the instability of *p*-DMAC provides an ideal solute model to verify the effectiveness of solvent induction modulation in reaction robustness. The present solvent induction strategy was verified to be effective in ng-level detection toward urea with a lifetime up to 346 h at 25 °C, which forms a sharp contrast with the original reaction expires shortly.

EXPERIMENTAL SECTION

Materials and Chemicals. Propanediol ($C_3H_8O_2$) and *p*-dimethylaminocinnamaldehyde ($C_{11}H_{13}NO$) were purchased from Aladdin Chemical Reagent, Ltd. Glycerol ($C_3H_8O_3$) and 2-propanol (C_3H_8O) were purchased from Tianjin Fengchuan Chemical Reagent Co., Ltd. Ultrapure deionized water (18 MΩ) was prepared by laboratory ultrapure water machine (water purifier, WP-UP-2). Concentrated sulfuric acid (H_2SO_4) was purchased from Sinopharm Chemical Reagent Co., Ltd. Porous sponges were purchased online from Alibaba. Unless otherwise noted, all reagents and materials were obtained from commercial sources, and all were used without further purification.

https://doi.org/10.1021/acs.analchem.2c00505
Anal. Chem. 2022, 94, 6318−6328

Instrumentation and Characterization. Ultraviolet−visible absorption spectra were measured on a grating spectrometer (Ocean Optics, Maya 2000 Pro). The dynamic color change and the dynamic particle diffusion process of the reactant on the reagent-endowed sponge were monitored by a video camera (Imavision, MER-2000-5GM/C-P) with a minimum resolution of 1.2 μm × 1.2 μm. The R/G/B value before or after reaction of reagent-endowed sponge and the time-varying diffusion diameters of urea microparticulate with different particle sizes were extracted using the Adobe Photoshop software. Field-emission scanning electron microscopy (FE-SEM, JEOL JSM-7610 F Plus, 4.0−6.0 kV) was used to characterize the morphology of the sponge. ATR-FTIR spectra were obtained using PerkinElmer Frontier with a universal ATR sampling accessory from PerkinElmer.

Preparation of Reagent and the Testing Process. The probe (*p*-dimethylaminocinnamaldehyde, $C_{11}H_{13}NO$, *p*-DMAC, 0.48 mg) was dissolved in 2 mL of solvent (water, 2-propanol, propanediol, and glycerol, respectively) with ultrasonication until a homogeneous solution was formed (1.37 mM), and then the obtained homogeneous mixed solution was added with the concentrated sulfuric acid (30 μL) while maintaining vigorous stirring. Three copies of each sample were prepared and then used to obtain the absorption spectra in different solvents.

Preparation of the Reagent-Endowed Sponge. The *p*-DMAC (0.48 mg) was dissolved in 5 mL of solvent (propanediol and glycerol, volume ratio 4:1) with ultrasonication until a homogeneous solution was formed (54.79 mM). Then, the obtained homogeneous mixed solution was added with concentrated sulfuric acid (300 μL) and stirred vigorously. Finally, the obtained reagent was immersed in a sponge made of polyurethane with an average pore size of 157 μm to construct the reagent-endowed sponge. The prepared reagent-endowed sponge was stuffed in a resin model for the convenience of testing and observation, in which the resin model was prepared by 3D printing.

Computation Method. The quantum chemical analysis in this work was performed by the Gaussian 09C,[48] and the wave function analysis was conducted by using the Multiwfn software.[49] The MD simulation was conducted by using the GROMACS package,[50] and the VMD 1.9.2 program[51] was used to plot the graph.

RESULTS AND DISCUSSION

Principle of the Proposed Solvent Induction Strategy for Survivable Colorimetric Detection. It is known that aldehyde group (−CHO), comprised of the carbonyl with α-H, is a highly reactive atomic group in the feature of positively charged carbon because of the greater electronegativity of oxygen than carbon, and has been endowed with many classical reactions, such as the Barbier reaction,[52] Strecker reaction,[53] Schiff base reaction,[54] and so on. However, a stubborn problem is the aldehyde group is prone to autoxidize and produce peracid, which would reversely react with aldehyde by nucleophilic attack if sufficient oxygen was provided, that is, continuously exposed in air (Figure 1a). With the emergence of the final acid product, the aldehyde group would be denatured and the designed reaction would be failed. Thus, the avoid of the autoxidation of aldehyde group is of great significance to maintain the preconceived performance and solvent which could prevent the autoxidation channel by blocking oxygen to directly contact with aldehyde group would be a possible choice. The detection of urea was selected to verify the blocking effect of the solvent for two reasons. One is that the detection of urea is meaningful in public security since urea could be prepared into an explosive with low friction sensitivity, low impact sensitivity, and strong explosive power of 90% TNT equivalent through quickly and easily mixing it with nitric acid in "back-yard" facilities. The other is that the primary amine ($-NH_2$) of urea could react with the aldehyde group through a classical Schiff base reaction, and more importantly, the formed imine is commonly a yellow color substance and could be directly observed. The *p*-DMAC, as a typical D-π-*A* molecule containing an aldehyde group and an "R" group consisting of a conjugated system with a benzene ring and a C=C bond, as well as strong electron-donating dimethylamino ($-N(CH_3)_2$), is an ideal model to intuitively investigate the solvent blocking effect with a more obvious color change due to the delocalized electron transfer from dimethylamino's nitrogen to imine through enlarged conjugated system. It could be clearly observed that if the solvent is water, *p*-DMAC denatured to acid that has a similar color signal with the urea detection product, which would seriously interfere with the authenticity of the colorimetric detection signal. However, a clear and noninterference rose-red signal could be observed if propanediol-glycerol solvent was adopted, indicating the validity of solvent blocking effect.

Considering the crucial role of the number of hydroxyl groups and the size of the hydrophobic alkyl part for choosing solvent, typically, water, 2-propanol, propanediol, and glycerol, were chosen to evaluate the corresponding influence on the solvent induction effect. To reflect the difference of Gibbs free energy barrier of detection reaction in different solvents, and thus to show the importance and effectiveness of solvent selection, the transition state analysis[55−57] of the reaction process between *p*-DMAC and urea was investigated. It can be seen that the nucleophilic reaction (R/1) forms the tetrahedral transition state and the leaving groups (in the form of dehydration) induce the configuration transformation (2/P) either in vacuum or in different solvents (Figure 1b). It is found that all the four solvents would not influence the reaction to form C−N bond (i.e., R/1), but all the four solvents could indeed decrease the Gibbs free energy barrier (ΔE) with about 20 kcal/mol, and propanediol does play the most significant role to make the reaction take place easier with a ΔE of 28.51 kcal/mol (Table S1). Moreover, the solvent could also indeed promote the dehydration reaction (i.e., 2/P), in which glycerol plays a more significant role with a ΔE of 46.55 kcal/mol.

It should be noted that solvent could not only act as a medium to directly participate in the reaction between the probe and the analyte, but also might to act on solute molecule to change its electronic structure and thus affect the sensing performance toward analyte. Through the analysis of the molecular configuration of *p*-DMAC, one can find that the dimethylamino group can rotate freely due to the single bond with the benzene ring, while the conjugated cinnamaldehyde can maintain relatively steady in-plane due to the extended p orbitals overlap from benzene ring to C=O bond (Figure 1c). Normally, the dominant electron cloud in the probe molecule is Π_6^6 formed by the benzene ring, in which the dimethylamino group is in a free rotation state and the N atom of it is sp^3 hybridized. Since the four hybrid orbitals of N atom form a tetrahedral structure, the dimethylamino group is favored to be vertical to form the minimum energy state

https://doi.org/10.1021/acs.analchem.2c00505
Anal. Chem. 2022, 94, 6318−6328

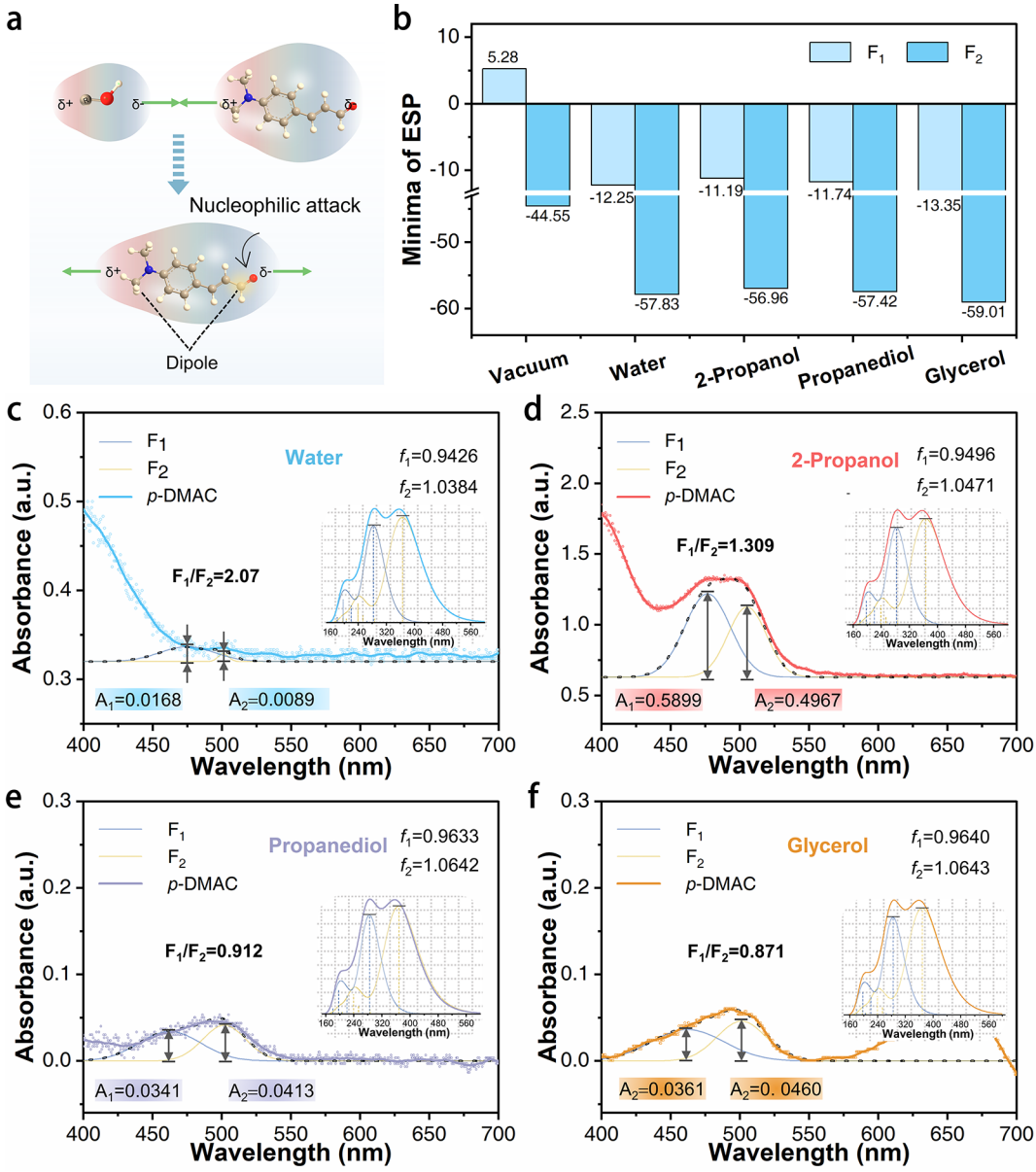

Figure 2. (a) Schematic illustration of the induction effect from the polar solvent on the probe molecule. (b) Histogram of the electrostatic potential (ESP) surface local minima and dipolemoment of F_1 and F_2 in vacuum and different solvents. Experimental and calculated UV−vis spectra of *p*-DMAC in (c) water, (d) 2-propanol, (e) propanediol, and (f) glycerol (f_1 and f_2 represent the oscillator strength of F_1 and F_2, respectively).

because the lone-pair electron of N atom is coplanar with the benzene ring, thus, this vertical configuration would exist in a high probability, nominally, Formation 1 (F_1). However, when the dimethylamino group is coplanar with the aromatic ring, the N atom of the and the dimethylamino α,β-unsaturated carbonyl bond located at the *para*-position group would be sp^2 hybridized would participate in the construction of π-conjugation to form a C═N bond and an enlarged π-conjugation Π_{10} [10], in which a higher partition function resulted from the high degree of electron delocalization and the low average electron kinetic energy would make the planar configuration, nominally, Formation 2 (F_2), highly probably exist. From the potential energy surface scan at dihedral angle of the two molecular configurations, it further confirms that when the dimethylamino group rotates to 90° or 270°, F_1 would be in the lowest energy state, while when the dimethylamino group rotates to 0° or 180°, F_2 would be in the lowest energy state. As a result, it would be of great significance to investigate whether solvent could facilitate the stable existence of these two configurations.

Influence of Solvent on Reactivity and Configuration Branching Ratio in Probe. Due to the induction force from the polar solvent, the dipolemoment of *p*-DMAC would increase, behaving as the more significant separation of positive and negative centers of molecules and the increased negative charge density of the oxygen (Figure 2a). The electron on the carbon atom of aldehyde group is more difficultly delocalize to the left fragment and thus the carbon atom would be vulnerable to be nucleophilically. Besides, the resulted reaction intermediate could be attacked stabilized by the polar solvent and make the reaction move forward, and thus improve the

https://doi.org/10.1021/acs.analchem.2c00505
Anal. Chem. 2022, 94, 6318−6328

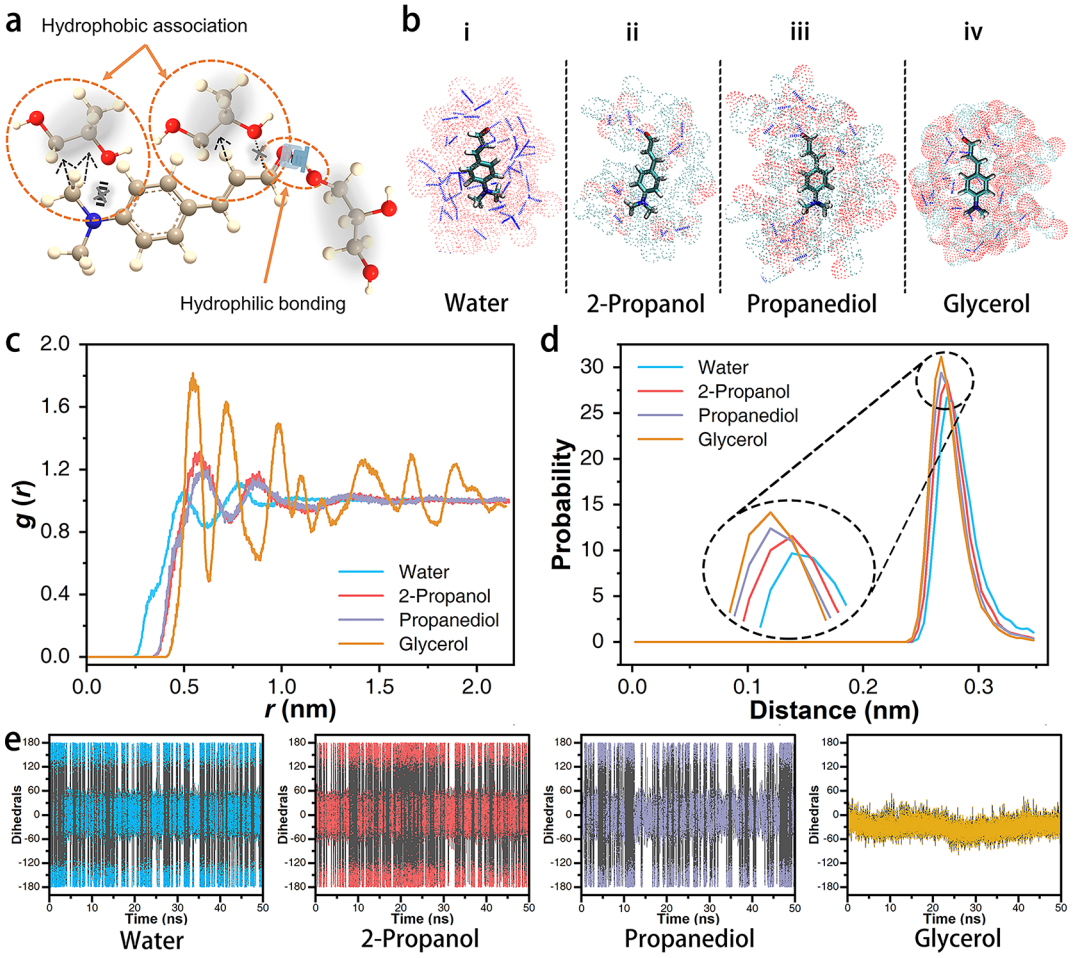

Figure 3. (a) Schematic illustration of the interaction between the hydrophobic shielding and hydrophilic bonding solvent cage and the effective interaction points in *p*-DMAC. (b) The solvent cage diagram consists of one *p*-DMAC around with solvent molecules in the range of 0.5 nm. (c) Radial distribution function ($g(r)$) of different solvent molecules with respect to *p*-DMAC. (d) The relationship of hydrogen bond probability and distance between solvents and solute. e) The statistical analysis at dihedral angle of *p*-DMAC in different solvents.

reaction activity of F_2 due to the plane-conjugated configuration which is beneficial to electron delocalization.

To achieve a better understanding on the solvent influence to the probe state, the two corresponding configurations and reactivity of *p*-DMAC were compared by electrostatic potential (ESP) analysis[58,59] (Figures S1 and S2). It can be obviously observed that the oxygen atom at aldehyde group owe a minimum ESP value in both F_1 and F_2 in vacuum, while this value in F_2 (−43.85 kcal/mol) is more negative than that in F_1 (4.93 kcal/mol), indicating that F_2 would have a much stronger electrostatic attraction to urea which is in favor of the nucleophilic attack of urea on the positively charged carbon in aldehyde group (Figure S3). It is found that although the ESP distribution of F_1 and F_2 does not change significantly in polar solvents such as water, 2-propanol, propanediol, and glycerol, the minimum ESP at the oxygen atom decreases, implying that the reaction activity would increase and the nucleophilic attack would happen more easily (Figures 2b and S4, Table S2). Upon careful comparison, it is found that due to the large dipole moment of F_1 and the more susceptible dipole−dipole interaction with solvent, the minimum ESP value in F_1 decreases about 4 more than that in F_2. However, the minimum ESP value in F_2 is always more negative than that in F_1, indicating that F_2 dominates the reaction. It could also be clearly observed that the minimum ESP value in F_1 and F_2 appear to be the most negative in glycerol, implying that the reaction activity of *p*-DMAC could be the largest in this polyhydroxy polar solvent.

When the electron arrangement and binding categories of the probe molecule changed, the configuration branching ratio of Formation 1 and Formation 2 (F_1/F_2) as an important parameter to determine the overall configuration distribution state of the probe would change consequently. In vacuum, the electron transition in F_1 and F_2 is generally forbidden to the first excited state and permitted to the second excited state (Table S3 and Figure S5). However, with the introduction of solvent, the transition in F_2 to the first and second excited states would be reversed. As a result, there would be an absorption peak appearing at a shorter wavelength position corresponding to the electron transition to the second excited state with an excited energy about 4.4 eV, while there would be an absorption peak appearing at a longer wavelength position corresponding to the electron transition to the first excited state with an excited energy about 3.4 eV. The absorption spectra of the two configurations in different solvents, including water, 2-propanol, propanediol, and glycerol, were measured to further investigate the effect of solvent on the configuration branching ratio of *p*-DMAC (Figure 2c−f). Based on the theoretical oscillator strength ratio (f_1/f_2) of the two configurations in a certain environment, and according to

https://doi.org/10.1021/acs.analchem.2c00505
Anal. Chem. 2022, 94, 6318−6328

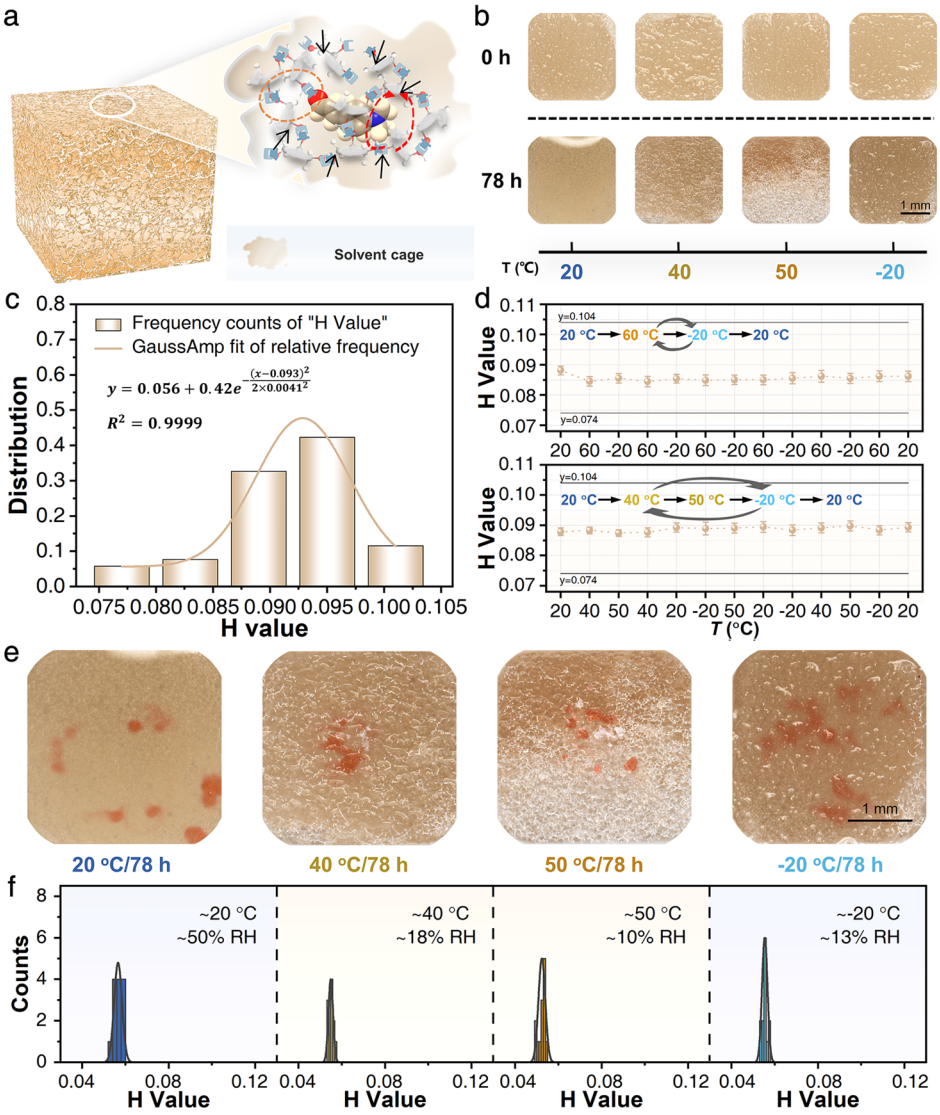

Figure 4. (a) Schematic diagram of the sensing platform constructed by the reagent-endowed sponge involving the solvent cage. (b) Images of the reagent-endowed sponges before and after exposing in air for 78 h at different temperatures (20, 40, 50, and −20 °C). (c) The histogram with the Gaussian fitting curve of the Hue (H) value taken randomly from different reagent-endowed sponges at different temperatures varying with time. (d) The change curve of the H value of the reagent-endowed sponges repeatedly or randomly changing the stocking temperature for the robustness evaluation. (e) The reaction color images of the reagent-endowed sponges toward urea after 78 h of storage at different temperatures. (f) The histograms of the H value taken randomly from the reagent-endowed sponges after reacted with urea at different temperatures varying with time.

the positive correlation between the configuration branching ratio and the absorption intensity ratio, the configuration branching ratio of *p*-DMAC in water, 2-propanol, propanediol, and glycerol could be obtained to be 2.07, 1.309, 0.912, and 0.871, respectively. It is clear that with the increase of the hydroxy number in solvent, the proportion of F_2 in the probe increases gradually and becomes dominant with the assistance of propanediol or glycerol. Thus, considering that more hydroxy groups and larger hydrophobic alkyl part of the solvent are more conducive to form effective solvation effects with *p*-DMAC, as well as facilitate the good solubility, propanediol−glycerol mixture with a typical volume ratio of 4 was chosen to achieve a favorable solvent environment to ensure the rapid sensing of *p*-DMAC.

Influence of Solvent Cage Constructed by Hydrophobic Shielding and Hydrophilic Bonding on Probe. The employment of propanediol-glycerol could also facilitate the building of solvent cage via hydrophobic shielding and hydrophilic bonding with the probe molecules to boost competitive delocalized charge transfer in quinone resonant *p*-DMAC (Figure 3a). Due to the steric hindrance, the hydrophobic shielding originated from the alkane part in the solvent molecule structure could weaken the electrostatic attraction between the positively charged carbon in the aldehyde group and the lone-pair electron at the oxygen atom in propanediol-glycerol. This hydrophobic shielding can also weaken the hydrogen-bond interaction between the nitrogen atom in the dimethylamino group and the hydrogen atom in hydroxyl group of the solvent molecule, and thus make the probe molecule maintain the original push−pull effect. At this time, the hydrophilic bonding originated from the hydroxyl part in the solvent molecule structure can form a strong hydrogen bond with the oxygen atom on the aldehyde group, which would make the push−pull effect of the probe

https://doi.org/10.1021/acs.analchem.2c00505
Anal. Chem. 2022, 94, 6318−6328

molecule be stronger, and thus the nitrogen atom in it would tend to be sp^2 hybridized, facilitating a decrease in the configuration branching ratio. This decrease trend would be more significant with the hydrophobic shielding and hydrophilic bonding effects simultaneously exist in the solvent cage.

To clearly illustrate how solvent would restrain the rotation of the dimethylamino group in the *p*-DMAC probe and result in a higher ratio of F_2, molecular dynamics (MD) simulation was performed to gain insights into the spatial distribution and hydrogen bond formation of the solvent molecules around *p*-DMAC, and further explain the influence of solvent cage on the molecular configuration at the molecular level (Figure S6). Four solvents environments, including water, 2-propanol, propanediol, and glycerol, were considered in a model that a cube box with side length of 4 nm filled with a *p*-DMAC placed in its center and different solvent molecules. It can be clearly observed with the solvent as water, *p*-DMAC could be densely wrapped with the solvent cage and the effective interaction points of it are closely contacted with the water molecules, resulting the weakening of the resonance ability of the probe molecule and thus a higher ratio of the F_1 in water (Figure 3b(i)).With the increase of the hydrophobic alkyl part in the solvent molecules, the force between the nitrogen atom in dimethylamino group and the carbon atom in aldehyde group with the solvent is weakened, resulting the increase of the resonance ability of the probe molecule and thus a higher ratio of the F_2 in 2-propanol, propanediol, and glycerol (Figure 3b(ii)−(iv)). Compare to the relatively looser 2-propanol cage, the dense propanediol or glycerol cage could not only further increase the resonance delocalization probability due to the enhanced hydrogen bond interaction probability between the polyhydroxy solvent molecule and the oxygen atom at the aldehyde group, but also restrain the rotation of the dimethylamino group in the *p*-DMAC probe, thus, resulting in an even higher ratio of F_2 in these two solvents.

The dimensional feature of the solvent cage could be directly expressed by the radial distribution function ($g(r)$) diagram, it can be seen that the distance of the first solvated shell of the four solvents shows an obvious difference with a distance from the central probe of 0.50, 0.56, 0.59, and 0.54 nm, respectively, corresponding to water, 2-propanol, propanediol, and glycerol (Figure 3c), indicating that the glycerol cage shrinks with more hydroxyl groups produced stronger intermolecular force. In addition, from the correlation diagram between hydrogen bond distance and probability, it is shown that propanediol and glycerol have shorter hydrogen bond distance and higher hydrogen bond probability compared with the other two solvents (Figure 3d), thus, the propanediol and glycerol environment would facilitate the stable bonding with the oxygen atom in aldehyde group. From the statistical analysis of the dihedral angle in different solvents (Figure 3e), it is clear that the with the increase of the hydrophobic alkyl part and the number of the hydroxyl groups, the rotation of the dimethylamino group in the *p*-DMAC probe would be further restrained through the observation of the decreased frequency. Especially, this roation could even be thoroughly restrained in glycerol due to the strong interaction between glycerol molecules. Thus, the propanediol-glycerol mixture solvent would greatly facilitate the existence of F_2 from the perspective of solvent cage. Thus, it is clearly demonstrated by computational simulations from quantum chemistry to molecular dynamics that solvent selection is important to make the recognition site (aldehyde group) more effective and to preferentially facilitate the existence of the planar configuration.

Robust Colorimetric Detection Brought by Solvent Induction Strategy. The propanediol-glycerol cage would allow one solvent molecule to bond simultaneously with the oxygen atom in *p*-DMAC and the other solvent molecules through hydrogen-bond interaction (Figure 4a). Thus, the effective interaction resulting from the strong hydrophobic and hydrophilic association in propanediol−glycerol would elevate the viscous drag of solvent. It is expected that the effective viscous drag between solvent cages within the solvent system could prevent the autoxidation channel of the aldehyde group, keeping the probe system being stable. To experimentally present the effectiveness of the solvent induction strategy, a polyurethane sponge medium with an average pore size of 157 μm was chosen to endow the reagent and construct a sensing platform to visibly show the dynamic color change toward urea solid particle (Figure S7). It is considered that the sponge is chemically stable to endow the reagent (Figure S8), and its flat surface is favorable for optical imaging. It could be seen intuitively that there is no obvious change in the original yellow-skin color even these pictures were taken randomly from different areas in different reagent-endowed sponges. After exposed in air for 78 h at different temperatures (20, 40, 50, and −20 °C), although the color of these four reagent-endowed sponges tends to turn a bit gray, which is proportional to the harsh temperature condition probably due to the evaporation difference, there is no distinct characteristic color appears (Figures 4b and S9).

The original color deviation could be numerically presented with the Hue (H) value from the images of the original reagent-endowed sponges (Figure 4c). It is clear that the value of H locates strictly in the range of 0.074 to 0.104 and centered at 0.093 with Gauss fitting, indicating that the yellow-skin color is very consistent, which would be beneficial for any color perturbation analysis. To exclude any unexpected disturbing to the color signal from reagent-endowed sponge itself to the temperature influence (Figure 4d), it was repeatedly put into an oven with 60 °C and a refrigerator with −20 °C for 10 min in each cycle and at least five cycles were adopted. It is found that the H value locates in the range of 0.088−0.084 with a perturbation of 0.003 throughout the whole process. Moreover, it is found that a random temperature treatment at 20, 40, 50, and −20 °C also has almost no influence to the H value (with a deviation of 0.001), indicating the perfect effect of the solvent induction strategy to the robustness of colorimetric sensing.

The protective effect of the solvent induction strategy was further verified by the effectiveness of the reaction toward urea after 78 h storage at different temperatures (Figures 4e and S10), representing with dotted brick-red color which is actually a mixture of the intrinsic rose-red and the background yellow-skin. The H value of this brick-red color locates in the range of 0.049−0.060 (Figure 4f), which is a very narrow range to distinguish the characteristic color with no disturbing from the influence of temperature, thus, intuitively expressed the reliability of the present solvent induction strategy.

To evaluate the possible improvement of the solvent induction strategy to the signal enhancement and long-time usage ability, the sensing performance of the reagent-endowed sponges toward urea particles was investigated. Furthermore, five categories of chemicals were selected for selectivity testing of the developed sensor, including nitrogen-containing

https://doi.org/10.1021/acs.analchem.2c00505
Anal. Chem. 2022, 94, 6318−6328

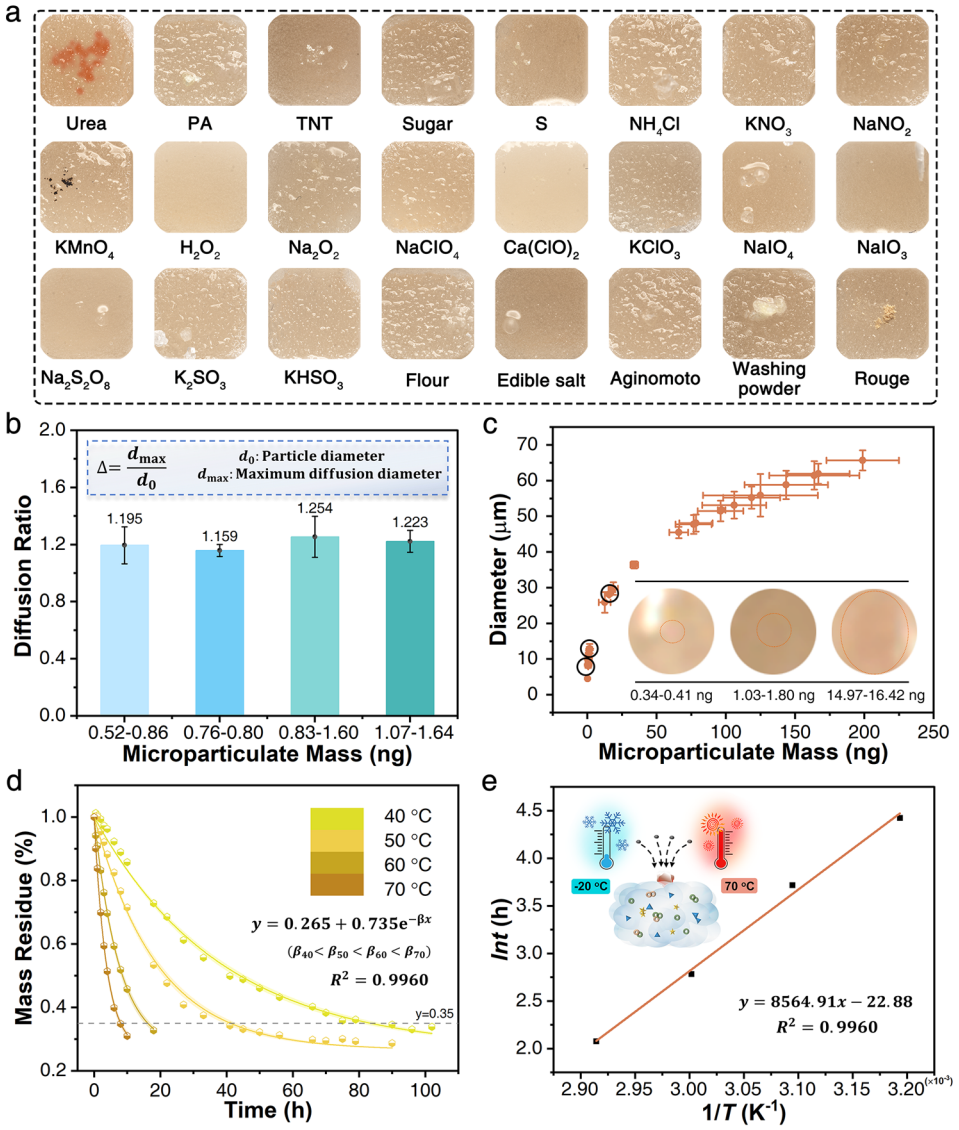

Figure 5. (a) Actual images of selectivity testing for the developed sensor to 23 interferents, including PA, TNT, sugar, S, NH_4Cl, KNO_3, $NaNO_2$, $KMnO_4$, H_2O_2, Na_2O_2, $NaClO_4$, $Ca(ClO)_2$, $KClO_3$, $NaIO_4$, $NaIO_3$, $Na_2S_2O_8$, K_2SO_3, $KHSO_3$, flour, edible salt, aginomoto, washing powder, and rouge. (b) Histogram of the ratio for the final diameter of the diffusion area to the particle diameter after 8.5 s. (c) The relationship between the amount of urea microparticulate and color change diameter. (d) Variation of the mass residue of the reagent-endowed sponges with time at different temperatures (40, 50, 60, and 70 °C). (e) The relationship between the lifetime of the reagent-endowed sponges and temperature deduced from the Arrhenius model.

explosives (PA and TNT), improvised explosives (sugar, S, NH_4Cl, KNO_3, $NaNO_2$, $KMnO_4$, H_2O_2, Na_2O_2, $NaClO_4$, $Ca(ClO)_2$, $KClO_3$), redox substances ($NaIO_4$, $NaIO_3$, $Na_2S_2O_8$, K_2SO_3, $KHSO_3$), and common daily products (flour, edible salt, aginomoto, washing powder, rouge; Figure 5a), there is no brick-red signal appears upon the detection of these interferents, implying the good selectivity of the developed sensor. From the perspective of the reaction mechanism, the detecting of urea by *p*-DMAC is based on Schiff base reaction between aldehyde group in the probe and the primary amine in urea, thus, other amine-containing molecules may react with *p*-DMAC in the same way theoretically. However, chemical colorimetry involves two processes, one is that the active center interacts strongly with analyte, and the other is to output this interaction by changing color. Amino group only satisfies the first process, and it is found th at aliphatic amines, including thiourea, acrylamide, glycine, L-cysteine, glutamic acid, and phenylalanine could not give characteristic color change whlie reacting with *p*-DMAC (Figure S11a). However, for aromatic amines, including *p*-anisidine, *p*-toluidine, aniline, *p*-fluoroanimine, sulfanilamide, and *p*-nitroaniline, they can also give red and purple color signals due to their relatively high activities (Figure S11b). Although these aromatic amines may interfere the characteristic color to urea, they are not commonly found in daily life and thus would not affect much on the sensing capability of the present sensing strategy to urea.

Urea is one typical improvised explosive, especially in the form of solid clusters in air or adhered on stuffs that can be easily desorbed with air exhausting by the explored detector for security checking. Thus, the most important sensing capability should be the minimal size or mass of a single microparticulate this method could realize. Urea microparticulate with different diameters suspended in a steady air flow were physically

https://doi.org/10.1021/acs.analchem.2c00505
Anal. Chem. 2022, 94, 6318−6328

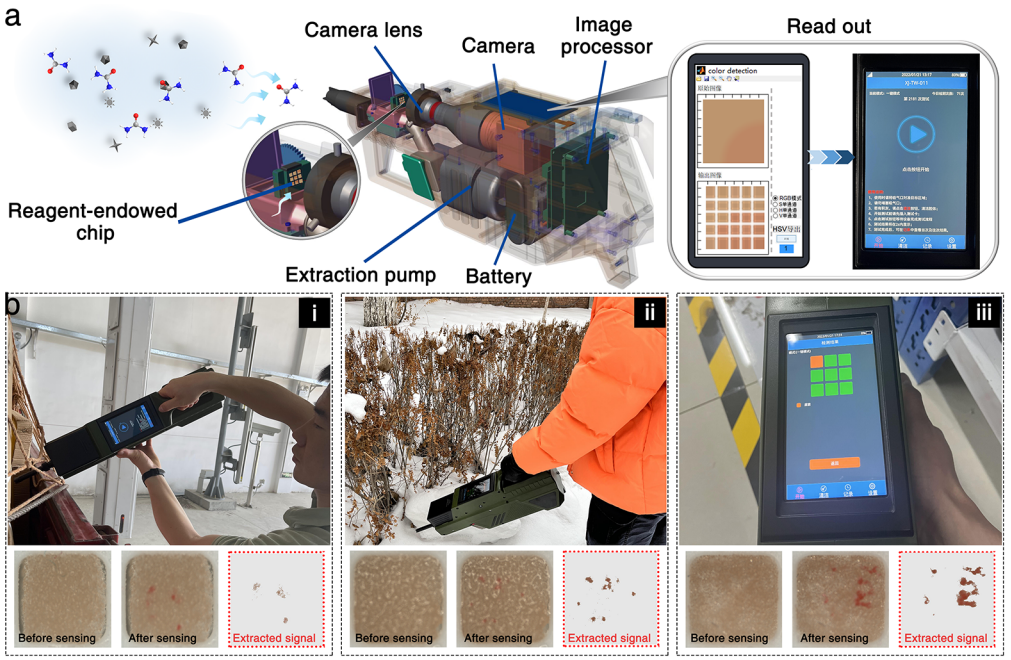

Figure 6. (a) Schematic of the working principle of a portable colorimetric detection platform. (b) Detection performance of the detection platform in real case (i: fresh sensing chip working at room temperature; ii: sensing chip strored at −20 °C for 1 h and working below 0 °C; iii: sensing chip strored at 60 °C for 4 h and working at room temperature).

adsorbed onto the surface of the reagent-endowed sponges to produce specific color changes for discrimination. It is expected that the solvent induction-promoted probe system would macroscopically being endowed with sensing signal concentrating ability and strong moisture retention capability due to the effective viscous drag.

The images for the detection of airborne urea microparticulate with different diameters were captured at the point where the initial color changes of the microparticulate could be discerned (Figure S12). One can see that the color change areas caused by the urea microparticulate with diameters ranging from 9.05 to 13.30 μm are visually discernible although there is a great influence from the urea crystal structure to the optical observation. It was found that the reaction speed was very fast from the extracted time-varying diffusion diameters of urea particles with different particle sizes (Figures 5b and S13), and although the diffusion diameters increase slowly with time, the ratio of the final diameter of the diffusion area to the particle diameter locates in the range of 1.16 to 1.25. Furthermore, from the roughly calculated relationship between the amount of urea microparticulate and the color change area (Figure 5c), the reagent-endowed sponge is capable of detecting very small microparticulate in amount as low as ng-level for urea, indicating that the viscous drag brought by the solvent induction strategy can effectively inhibit the diffusion of the color signal and promote the real detection ability.

Generally, the *p*-DMAC probe could only be effective to detect urea in air within 2 h at 40 °C without any solvent induction design. However, it is found that with the present solvent induction strategy, although the mass residue of the reagent-endowed sponges exponentially decreases with time at different temperatures, they are capable of detecting urea for at least 84, 41, 16, and 8 h when exposing in air at elevated temperatures of 40, 50, 60, and 70 °C (Figure 5d). If we take 35% mass residue as the basic effective standard to evaluate the lifetime of the reagent-endowed sponge, it could be calculated from the Arrhenius model that the lifetime is up to 346 h when exposed in air at a room temperature of 25 °C (Figure 5e and Table S4), which actually corresponds well with the real situation of a lifetime of over 400 h at room temperature at a RH of 26% (Figure S14). This result further proves that the hydrophobic shielding and hydrophilic bonding solvent cage strategy could be a very effective methodology for the design of colorimetric reagent for highly survivable and endurable sensing with ultrasensitive detection capability.

Portable Detection Platform for Rapid, On-Site, and Survivable Colorimetric Urea Sensing. To further prove the applicability of the proposed solvent induction strategy for the rapid, on-site, and survivable colorimetric detection of urea, a portable detection platform consisting of a camera, camera lens, image processor, extraction pump, battery, and a reagent-endowed chip is constructed (Figure 6a), in which the image processor implanted with special algorithm could perform the image segmentation based on the color (HSV value) threshold and extract the specific value from instant captured images to accurately judge the detection results.

To evaluate the sensing performance of the fresh sensing chip working in real case at room temperature, the portable detection platform was applied in simulated scenarios with suspected urea microparticulates suspending in air (Figure 6b(i)). A distinct brick-red signal region could be discerned by subtracting the original image with the one after detection. It should be noted that the diffusion of the generated color signal is very limited since it would take at least 4 s for the urea microparticulates transporting through the chamber to the chip together with the feedback time, demonstrating the superior signal concentrating ability originated from the solvent induction strategy. Besides, a total detection time period of 4 s is of great attractiveness to facilitate on-site detection. To further investigate whether the sensing chip is robust enough to experience cold or hot inflicted conditions in practical

https://doi.org/10.1021/acs.analchem.2c00505
Anal. Chem. 2022, 94, 6318−6328

situlation, the sensing chip was first stored at −20 °C for 1 h or at 60 °C for 4 h and then working on the portable detection platform below 0 °C or at room temperature (Figure 6b(ii) and (iii)). Under both situations, the intrinsic brick-red signal could be constrained distinctively in fixed dotted areas with an obvious boundary, confirming the strong tolerance of the sensing chip. Besides, it should be noted that in the real case, the sensing chip would suffer from the temperature elevating accelerated aging due to the consistent pumping. However, the sensing chip still exhibits a rapid and accurate performance with an intermittent working after 8 h in the real case, demonstrating the great superiorities of the competitive delocalized charge transfer boosted by solvent induction strategy for survivable colorimetric sensing.

Compared with the previously reported sensors, the present sensor shows superioties in selectivity, sensibility, and reproducibility (Table S5), proving the reasonability of the solvent induction strategy for enhancing the overall sensing performance. Furthermore, the sensing unit in the developed sensor is disposable due to the reaction principle of chemical colorimetry, which is also shown in Table S5. However, it should be noted that the sensing unit is allowed for long-term monitoring for up to 346 h at room temperature when equipped into the detector if there is no urea detected, and once positive alarming is triggered, it should be disposed.

CONCLUSIONS

In conclusion, the proposed solvent induction strategy involving a hydrophobic shielding and hydrophilic bonding solvent cage allows the stable existence of a highly active configuration in the reagent for highly survivable and endurable sensing with high sensitivity toward the urea microparticulate. The synergy of the hydrophobic shielding from the alkyl part and the hydrophilic bonding from the polyhydroxy could boost the competitive delocalized charge transfer in *p*-DMAC and elevate the viscous drag in the reagent, thus endowing the reagent-endowed sponges with a sensing signal concentrating ability and a moisture retention capability. This solvent induction strategy was further intuitively evidenced by the little color signal perturbation of the original reagent-endowed sponges and the distinct and consistent color signal after the reaction, as well as the detection capability at the ng-level and a lifetime of up to 346 h at 25 °C. Furthermore, the applicability of the proposed solvent induction strategy for the rapid, on-site, and survivable colorimetric detection of urea was proved by the exploration of a portable detection platform with promising utilization. We expect this tentative study will not only pave a new way for accurate and reliable chemical sensing and shine light on the development of high-performance sensors, but also be favorable for promoting the activity and stability of D-π-*A* molecules from the perspective of solvent selection.

ASSOCIATED CONTENT

Supporting Information

The Supporting Information is available free of charge at https://pubs.acs.org/doi/10.1021/acs.analchem.2c00505.

Sensing performance testing, computation details, and the corresponding charts and tables associated with the manuscript (PDF)

AUTHOR INFORMATION

Corresponding Author

Xincun Dou − *Xinjiang Key Laboratory of Explosives Safety Science, Xinjiang Technical Institute of Physics and Chemistry, Chinese Academy of Sciences, Urumqi 830011, China; Center of Materials Science and Optoelectronics Engineering, University of Chinese Academy of Sciences, Beijing 100049, China;* orcid.org/0000-0001-5825-9937; Email: xcdou@ms.xjb.ac.cn

Authors

Xiaoyun Hu − *Xinjiang Key Laboratory of Explosives Safety Science, Xinjiang Technical Institute of Physics and Chemistry, Chinese Academy of Sciences, Urumqi 830011, China; Center of Materials Science and Optoelectronics Engineering, University of Chinese Academy of Sciences, Beijing 100049, China*

Tianshi Zhang − *Xinjiang Key Laboratory of Explosives Safety Science, Xinjiang Technical Institute of Physics and Chemistry, Chinese Academy of Sciences, Urumqi 830011, China; Center of Materials Science and Optoelectronics Engineering, University of Chinese Academy of Sciences, Beijing 100049, China*

Jiguang Li − *Xinjiang Key Laboratory of Explosives Safety Science, Xinjiang Technical Institute of Physics and Chemistry, Chinese Academy of Sciences, Urumqi 830011, China; Center of Materials Science and Optoelectronics Engineering, University of Chinese Academy of Sciences, Beijing 100049, China*

Zhiwei Ma − *Xinjiang Key Laboratory of Explosives Safety Science, Xinjiang Technical Institute of Physics and Chemistry, Chinese Academy of Sciences, Urumqi 830011, China; Center of Materials Science and Optoelectronics Engineering, University of Chinese Academy of Sciences, Beijing 100049, China*

Da Lei − *Xinjiang Key Laboratory of Explosives Safety Science, Xinjiang Technical Institute of Physics and Chemistry, Chinese Academy of Sciences, Urumqi 830011, China*

Baiyi Zu − *Xinjiang Key Laboratory of Explosives Safety Science, Xinjiang Technical Institute of Physics and Chemistry, Chinese Academy of Sciences, Urumqi 830011, China*

Complete contact information is available at: https://pubs.acs.org/10.1021/acs.analchem.2c00505

Author Contributions

The manuscript was written through contributions of all authors. All authors have given approval to the final version of the manuscript.

Author Contributions

#These authors contributed equally.

Notes

The authors declare no competing financial interest.

ACKNOWLEDGMENTS

This work was supported by the West Light Foundation of the Chinese Academy of Sciences (CAS Grant No. 2020-XBQNXZ-022), National Natural Science Foundation of China (21974150, U1903306), the Youth Innovation Promotion Association, CAS (NO. 2018474), Key Research Program of Frontier Sciences (CAS Grant No. ZDBS-LY-

JSC029), and Natural Science Foundation of Xinjiang (2022D01E03).

REFERENCES

(1) Yetisen, A. K.; Moreddu, R.; Seifi, S.; Jiang, N.; Vega, K.; Dong, X.; Dong, J.; Butt, H.; Jakobi, M.; Elsner, M.; Koch, A. W. *Angew. Chem., Int. Ed.* **2019**, *58*, 10506−10513.
(2) Matzeu, G.; Naveh, G. R. S.; Agarwal, S.; Roshko, J. A.; Ostrovsky-Snider, N. A.; Napier, B. S.; Omenetto, F. G. *Adv. Sci.* **2021**, *8*, 2003416.
(3) Bergua, J. F.; Alvarez-Diduk, R.; Idili, A.; Parolo, C.; Maymo, M.; Hu, L.; Merkoci, A. *Anal. Chem.* **2022**, *94*, 1271−1285.
(4) Lin, C.; Du, Z.; Tao, N.; Wang, D. *ACS Sens* **2021**, *6*, 439−442.
(5) Liu, B.; Zhuang, J.; Wei, G. *Environ. Sci. Nano* **2020**, *7*, 2195−2213.
(6) Feng, L.; Musto, C. J.; Suslick, K. S. *J. Am. Chem. Soc.* **2010**, *132*, 4046−4047.
(7) Guo, L.; Wang, T.; Wu, Z.; Wang, J.; Wang, M.; Cui, Z.; Ji, S.; Cai, J.; Xu, C.; Chen, X. *Adv. Mater.* **2020**, *32*, 2004805.
(8) Kaur, M.; Harpaz, D.; Eltzov, E. *Sens. Actuators B Chem.* **2022**, *356*, 131354.
(9) Wang, G.; Li, Y.; Cai, Z.; Dou, X. *Adv. Mater.* **2020**, *32*, 1907043.
(10) Wang, G.; Cai, Z.; Dou, X. *Cell Rep. Phys. Sci.* **2021**, *2*, 100317.
(11) Zhao, M.; Yu, H.; He, Y. *Sens. Actuators B Chem.* **2019**, *283*, 329−333.
(12) Chen, L.; Wu, D.; Kim, J. M.; Yoon, J. *Anal. Chem.* **2017**, *89*, 12596−12601.
(13) Sun, Y.; Wang, Y.; Cao, D.; Chen, H.; Liu, Z.; Fang, Q. *Sens. Actuators B Chem.* **2012**, *174*, 500−505.
(14) Bian, Y.; Wang, Y.; Yuan, H.; Bao, G.-M.; Su, D. *Dyes. Pigm.* **2022**, *198*, 110009.
(15) Huang, Y.; Zhang, Y.; Huo, F.; Chao, J.; Cheng, F.; Yin, C. *J. Am. Chem. Soc.* **2020**, *142*, 18706−18714.
(16) Goudappagouda; Dongre, S. D.; Das, T.; Santhosh Babu, S. *J. Mater. Chem. A* **2020**, *8*, 10767−10771.
(17) Wang, F.; Wang, L.; Chen, X.; Yoon, J. *Chem. Soc. Rev.* **2014**, *43*, 4312.
(18) Wei, P.; Liu, L.; Wen, Y.; Zhao, G.; Xue, F.; Yuan, W.; Li, R.; Zhong, Y.; Zhang, M.; Yi, T. *Angew. Chem., Int. Ed.* **2019**, *58*, 4547−4551.
(19) Chen, X.; Wang, F.; Hyun, J. Y.; Wei, T.; Qiang, J.; Ren, X.; Shin, I.; Yoon, J. *Chem. Soc. Rev.* **2016**, *45*, 2976−3016.
(20) Zhang, X.; Yang, Q.; Lang, Y.; Jiang, X.; Wu, P. *Anal. Chem.* **2020**, *92*, 12400−12406.
(21) Liu, C.; Liu, J.; Zhang, W.; Wang, Y. L.; Liu, Q.; Song, B.; Yuan, J.; Zhang, R. *Adv. Sci.* **2020**, *7*, 2000458.
(22) Su, Z.; Li, Y. S.; Li, J. G.; Dou, X. C. *Sens. Actuators B Chem.* **2021**, *336*, 129728.
(23) Zheng, P.; Cui, Z. Y.; Liu, H. C.; Cao, W. J.; Li, F.; Zhang, M. *J. Hazard. Mater.* **2021**, *415*, 125619.
(24) Qian, S.; Sun, S.; Wang, Y.; Li, Z.; Lin, H. *Sci. China Chem.* **2019**, *62*, 1601−1618.
(25) Tarai, A.; Li, Y.; Liu, B.; Zhang, D.; Li, J.; Yan, W.; Zhang, J.; Qu, J.; Yang, Z. *Coord. Chem. Rev.* **2021**, *445*, 214070.
(26) Feng, Y.; Wang, Y.; Ying, Y. *Coord. Chem. Rev.* **2021**, *446*, 214102.
(27) Abdul-Karim, N.; Blackman, C. S.; Gill, P. P.; Morgan, R. M.; Matjacic, L.; Webb, R.; Ng, W. H. *Anal. Chem.* **2016**, *88*, 3899−3908.
(28) Vermeij, E.; Duvalois, W.; Webb, R.; Koeberg, M. *Forensic Sci. Int.* **2009**, *186*, 68−74.
(29) Peng, L.; Hua, L.; Wang, W.; Zhou, Q.; Li, H. *Sci. Rep.* **2015**, *4*, 6631.
(30) Ma, Z.; Li, J.; Hu, X.; Cai, Z.; Dou, X. *Adv. Sci.* **2020**, *7*, 2002991.
(31) Mako, T. L.; Levenson, A. M.; Levine, M. *ACS Sens* **2020**, *5*, 1207−1215.
(32) Shojaeifard, Z.; Hemmateenejad, B. *Sens. Actuators B Chem.* **2022**, *356*, 131379.
(33) Wang, P.; Cai, Z.; Li, J.; Li, Y.; Zu, B.; Dou, X. *Adv. Optical Mater.* **2020**, *8*, 2000524.
(34) Bakshi, S.; Snoswell, A. J.; Kwok, K. Y.; Cheng, L. H.; Altalhi, T. A.; Santos, A.; Popat, A.; Kumeria, T. *Adv. Funct. Mater.* **2022**, 2103496.
(35) Lee, H.; Lee, J.; Lee, S.-G.; Doyle, P. S. *Anal. Chem.* **2020**, *92*, 5750−5755.
(36) Roh, Y. H.; Lee, H. J.; Kim, J. Y.; Kim, H. U.; Kim, S. M.; Bong, K. W. *Lab Chip* **2020**, *20*, 2841−2850.
(37) Hu, X.; Ma, Z.; Li, J.; Cai, Z.; Li, Y.; Zu, B.; Dou, X. *Mater. Horiz.* **2020**, *7*, 3250−3257.
(38) Ariga, K.; Ito, H.; Hill, J. P.; Tsukube, H. *Chem. Soc. Rev.* **2012**, *41*, 5800−5835.
(39) Gu, Y. *Green Chem.* **2012**, *14*, 2091−2128.
(40) Reichardt, C.; Welton, T. *Solvents and Solvent Effects in Organic Chemistry*: Fourth ed., Wiley-VCH, 2010; pp 65−99.
(41) Payehghadr, M.; Hashemi, S. E. *J. Incl. Phenom. Macrocycl. Chem.* **2017**, *89*, 253−271.
(42) Yu, P.; Zhai, Y.; Bao, R.-Y.; Liu, Z.-Y.; Yang, M.-B.; Yang, W. *Sens. Actuators B Chem.* **2019**, *299*, 126948.
(43) Liu, Y.; Li, J.; Wang, G.; Zu, B.; Dou, X. *Anal. Chem.* **2020**, *92*, 13980−13988.
(44) Swain, C. G.; Eddy, R. W. *J. Am. Chem. Soc.* **1948**, *70*, 2989−2994.
(45) Henkel, S.; Misuraca, M. C.; Ding, Y.; Guitet, M.; Hunter, C. A. *J. Am. Chem. Soc.* **2017**, *139*, 6675−6681.
(46) Adams, J. S.; Chemburkar, A.; Priyadarshini, P.; Ricciardulli, T.; Lu, Y.; Maliekkal, V.; Sampath, A.; Winikoff, S.; Karim, A. M.; Neurock, M.; Flaherty, D. W. *Science* **2021**, *371*, 626−632.
(47) Mellmer, M. A.; Sanpitakseree, C.; Demir, B.; Bai, P.; Ma, K.; Neurock, M.; Dumesic, J. A. *Nat. Catal.* **2018**, *1*, 199−207.
(48) Frisch, M. J.; Trucks, G. W.; Schlegel, H. B.; Scuseria, G. E.; Robb, M. A.; Cheeseman, J. R.; Scalmani, G.; Barone, V.; Petersson, G. A.; Nakatsuji, H.; Li, X.; Caricato, M.; Marenich, A. V.; Bloino, J.; Janesko, B. G.; Gomperts, R.; Mennucci, B.; Hratchian, H. P.; Ortiz, J. V.; Izmaylov, A. F.; Sonnenberg, J. L.; Williams; Ding, F.; Lipparini, F.; Egidi, F.; Goings, J.; Peng, B.; Petrone, A.; Henderson, T.; Ranasinghe, D.; Zakrzewski, V. G.; Gao, J.; Rega, N.; Zheng, G.; Liang, W.; Hada, M.; Ehara, M.; Toyota, K.; Fukuda, R.; Hasegawa, J.; Ishida, M.; Nakajima, T.; Honda, Y.; Kitao, O.; Nakai, H.; Vreven, T.; Throssell, K.; Montgomery, J. A., Jr.; Peralta, J. E.; Ogliaro, F.; Bearpark, M. J.; Heyd, J. J.; Brothers, E. N.; Kudin, K. N.; Staroverov, V. N.; Keith, T. A.; Kobayashi, R.; Normand, J.; Raghavachari, K.; Rendell, A. P.; Burant, J. C.; Iyengar, S. S.; Tomasi, J.; Cossi, M.; Millam, J. M.; Klene, M.; Adamo, C.; Cammi, R.; Ochterski, J. W.; Martin, R. L.; Morokuma, K.; Farkas, O.; Foresman, J. B.; Fox, D. J. *Gaussian 09*, Revision C.01; Gaussian: Wallingford, CT, 2016.
(49) Lu, T.; Chen, F. W. *J. Comput. Chem.* **2012**, *33*, 580−592.
(50) Abraham, M. J.; Murtola, T.; Schulz, R.; Pall, S.; Smith, J. C.; Hess, B.; Lindahl, E. *Softwarex* **2015**, *1*−*2*, 19−25.
(51) Humphrey, W.; Dalke, A.; Schulten, K. J. j. m. g. *J. Mol. Graph. Model.* **1996**, *14*, 33−38.
(52) Sun, X. L.; Liu, D. M.; Tian, D.; Zhang, X. Y.; Wu, W.; Wan, W. M. *Nat. Commun.* **2017**, *8*, 1210.
(53) Liu, W.; Yu, Z.; Winssinger, N. *Org. Lett.* **2021**, *23*, 969−973.
(54) Wang, L.; Hou, Y.; Zhong, X.; Hu, J.; Shi, F.; Mi, H. *Carbohydr. Polym.* **2019**, *208*, 42−49.
(55) Van Duin, A. C.; Zeiri, Y.; Dubnikova, F.; Kosloff, R.; Goddard, W. A. *J. Am. Chem. Soc.* **2005**, *127*, 11053−11062.
(56) Rousseaux, S.; Gorelsky, S. I.; Chung, B. K.; Fagnou, K. *J. Am. Chem. Soc.* **2010**, *132*, 10692−10705.
(57) Beaumont, M.; Jusner, P.; Gierlinger, N.; King, A. W. T.; Potthast, A.; Rojas, O. J.; Rosenau, T. *Nat. Commun.* **2021**, *12*, 2513.
(58) Murray, J. S.; Politzer, P. *WIREs Comput. Mol. Sci.* **2011**, *1*, 153−163.
(59) Suresh, C. H.; Remya, G. S.; Anjalikrishna, P. K. *WIREs Comput. Mol. Sci.* **2022**, *2022*, e1601.

https://doi.org/10.1021/acs.analchem.2c00505
Anal. Chem. 2022, 94, 6318−6328